

# MEASURING THE FRACTION OF OBSCURED QUASARS BY THE INFRARED LUMINOSITY OF UNOBSCURED QUASARS

EZEQUIEL TREISTER,<sup>1</sup> JULIAN H. KROLIK,<sup>2</sup> AND CORNELIS DULLEMOND<sup>3</sup>

*ApJ Accepted, Jan. 23 2008*

## ABSTRACT

Recent work has suggested that the fraction of obscured AGN declines with increasing luminosity, but it has been difficult to quantify this trend. Here, we attempt to measure this fraction as a function of luminosity by studying the ratio of mid-infrared to intrinsic nuclear bolometric luminosity in unobscured AGN. Because the mid-infrared is created by dust reprocessing of shorter wavelength nuclear light, this ratio is a diagnostic of  $f_{\text{obsc}}$ , the fraction of solid angle around the nucleus covered by obscuring matter. In order to eliminate possible redshift-dependences while also achieving a large dynamic range in luminosity, we have collected archival 24 micron MIPS photometry from objects with  $z \sim 1$  in the Sloan Digital Sky Survey (SDSS), the Great Observatories Origins Deep Survey (GOODS) and the Cosmic Evolution Survey (COSMOS). To measure the bolometric luminosity for each object, we used archival optical data supplemented by GALEX data. We find that the mean ratio of 24  $\mu\text{m}$  to bolometric luminosity decreases by a factor of  $\sim 3$  in the  $L_{\text{bol}} = 10^{44} - 3 \times 10^{47}$  ergs  $\text{s}^{-1}$  range, but there is also a large scatter at constant  $L_{\text{bol}}$ . Using radiation transfer solutions for model geometries, we show how the IR/bolometric ratio relates to  $f_{\text{obsc}}$  and compare these values with those obtained from samples of X-ray selected AGN. Although we find approximate agreement, our method indicates somewhat higher values of  $f_{\text{obsc}}$ , particularly in the middle range of luminosities, suggesting that there may be a significant number of heavily obscured AGN missed by X-ray surveys.

*Subject headings:* galaxies: active – quasars: general – infrared: galaxies

## 1. UNIFIED AGN SCHEMES AT LOW LUMINOSITY

Following the initial recognition by Antonucci & Miller (1985) that the nucleus of the prototypical type 2 Seyfert galaxy NGC 1068 must be surrounded by a toroidal belt of gas and dust, a tremendous amount of evidence has accumulated in support of the idea that similar obscuring tori surround the nuclei of other type 2 Seyfert galaxies (as reviewed, for example, in Antonucci 1993; Krolik 1999). Spectropolarimetry (the method originally employed by Antonucci and Miller) applied to both type 2 Seyfert galaxies and radio galaxies (di Serego Alighieri et al. 1994) often reveals in polarized light broad optical/UV emission lines and a strong non-stellar continuum that are essentially invisible in the total flux spectrum. In many examples of both these types of AGN, conical regions of bright line emission from highly-ionized elements point at the otherwise obscured nucleus (Ferruit et al. 2000; Schmitt et al. 2003). Similarly, both type 2 Seyfert galaxies and radio galaxies often exhibit X-ray continua that either show evidence for very large column densities of material along the line of sight or are extremely weak, likely indicating that the obscuration is Compton thick (Risaliti et al. 1999; Treister et al. 2004). In two cases, NGC 1068 and the Circinus galaxy, the obscuring torus can be seen directly in interferometric infrared imaging (Jaffe et al. 2004; Tristram et al. 2007).

The principal effect of this toroidal obscuration is that

observers trying to see the nucleus along lines of sight that pass through it are prevented from seeing anything but dust-reprocessed infrared continuum and (perhaps) hard X-rays. Consequently, most of the classic signatures of AGN—broad optical/UV emission lines, strong optical/UV non-stellar continuum, strong X-ray continuum—are obliterated when the object is seen from such a direction. Only when the line of sight passes through the central hole of the torus can all these features be seen, and the object is perceived as a type 1 AGN.

In the nearby Universe, where we can see large numbers of low luminosity AGN, large statistical samples have been assembled in order to measure the luminosity functions of both type 1 and type 2 AGN. Ideally compared at matched bolometric luminosity, but more often in terms of their luminosity in a single band or feature, the ratio of their numbers can be immediately interpreted as the ratio of unobscured to obscured solid angle. For example, Hao et al. (2005) and Simpson (2005), using samples of optically-selected AGN from the Sloan Digital Sky Survey, found that the ratio of type 1 objects to type 2 objects increases with increasing luminosity, from  $\simeq 2/3$  at an [OIII] 5007 luminosity of  $10^6 L_{\odot}$  to  $\simeq 2$  for line luminosities  $\sim 3 \times 10^7 L_{\odot}$ . Using samples of X-ray selected AGN, Steffen et al. (2003) and Barger et al. (2005) argued for a similar shift in the ratio of unobscured to obscured, suggesting that the unobscured variety come to dominate the total population for 2–8 keV luminosity  $\gtrsim 10^{44}$  erg  $\text{s}^{-1}$ . Similar results were obtained by Ueda et al. (2003), La Franca et al. (2005) and others, also using X-ray selected AGN samples. In fact, hints of such a trend were already seen in the much smaller 3CR radio sample Lawrence (1991).

However, there remain significant uncertainties in the

<sup>1</sup> European Southern Observatory, Casilla 19001, Santiago 19, Chile. Email: etreiste@eso.org

<sup>2</sup> Department of Physics and Astronomy, Johns Hopkins University, 3400 North Charles Street, Baltimore, MD 21218-2686. Email: jhk@pha.jhu.edu

<sup>3</sup> Max-Planck-Institut für Astronomie, Königstuhl 17, 69117 Heidelberg, Germany. Email: dullemon@mpia.de

measured population ratio at high luminosity. For example, Compton-thick AGN are completely missing from X-ray-selected samples. Other sample construction methods (e.g., the very large sample of type 2 quasars selected from the SDSS based primarily on [OIII] emission by Zakamska et al. 2003) can potentially yield quantitative estimates of comparative luminosity functions, but require substantial work in order to turn catalogs into space densities. Although much effort has been made in the last few years to construct AGN samples from mid-infrared observations with the *Spitzer Space Telescope*, the selection effects remain too poorly understood and the sample size is sometimes too small to permit extraction of a trend in the type ratio as a function of luminosity (Stern et al. 2005; Alonso-Herrero et al. 2006; Martínez-Sansigre et al. 2006; Lacy et al. 2007).

Here we attempt a different approach to the problem of measuring the unobscured/obscured ratio: using the ratio of reradiated mid-infrared continuum to bolometric luminosity in type 1 AGN as a surrogate (cf. the suggestions in Lawrence 1991; Barger et al. 2005). Because the obscuration transforms essentially all the nuclear radiation incident upon it into mid-infrared continuum via dust reradiation, and detailed radiation transfer calculations suggest that most of that continuum is radiated toward observers in the type 1 direction no matter what the detailed arrangement of dust may be (Pier & Krolik 1992; Granato & Danese 1994; Efstathiou & Rowan-Robinson 1995; Nenkova et al. 2002; van Bemmél & Dullemond 2003; Dullemond & van Bemmél 2005), this ratio should give a good indicator of the ratio of unobscured/obscured solid angle. The relative ease of identifying type 1 AGN across a wide dynamic range in luminosity also gives this method a number of advantages relative to those dependent on actually counting type 2 objects. Maiolino et al. (2007) have recently made an effort to implement this program, but the details of their method differ in significant ways from ours; we will comment on specific contrasts as they arise.

This paper is structured as follows: In section §2 we present the selection criteria and basic observational properties of the sources used in this work. In section §3 we study the correlations found in this sample, while the significance and interpretation of these trends are discussed in §4. Our conclusions are presented in §5. When required, we assume a  $\Lambda$ CDM cosmology with  $h_0=0.71$ ,  $\Omega_m=0.3$  and  $\Omega_\Lambda=0.7$ , in agreement with the most recent cosmological observations (Spergel et al. 2007).

## 2. SAMPLE DEFINITION AND DATA SOURCES

In order to eliminate any possibility that what we find involves an evolutionary effect rather than a luminosity dependence, we chose a sample of AGN that all have nearly the same redshift ( $0.8 \leq z \leq 1.2$ ), in contrast with the Maiolino et al. (2007) sample which includes sources at all redshifts. This particular redshift is a convenient choice because it is large enough that luminous quasars were common, but not so large that low luminosity AGN are too faint to detect. To achieve the greatest possible dynamic range in luminosity, we made use of three samples with complementary properties: one that has very large solid angle but is relatively shallow (Sloan Digital Sky Survey: SDSS), one that has smaller solid angle but

goes deeper (Great Observatories Origins Deep Survey: GOODS) and one intermediate approach (Cosmic Evolution Survey: COSMOS).

For our infrared band, we used the Spitzer Space Telescope MIPS  $24\mu\text{m}$  channel. The corresponding rest-frame wavelengths are  $\simeq 12\mu\text{m}$ ; by requiring  $z \leq 1.2$ , we avoid most of the contamination from the  $9.7\mu\text{m}$  silicate feature. For the highest redshift sources, this silicate feature can influence our  $24\mu\text{m}$  photometry, however this will affect only a small fraction of our sample. In addition, at this relatively short wavelength, stellar-heated dust is usually relatively faint. From the composite QSO spectrum with individually detected PAH features of Schweitzer et al. (2006; Figure 2 top panel), we can estimate the fraction of integrated flux contributed by the  $11.3\mu\text{m}$  PAH feature in the MIPS 24 micron band at  $0.8 < z < 1.2$ , and we find a maximum contribution of only 1.3%; hence this contribution is completely negligible. Moreover, because we use only unobscured AGN with  $L_{\text{bol}}$  from  $10^{44}$  to  $10^{47.5}$  ergs  $\text{s}^{-1}$ , stellar heating is unlikely to be a significant contaminant. The AGN from the SDSS were selected based on their optical properties, while in the case of the GOODS and COSMOS sources they were X-ray selected. In any case, the selection is completely independent of their infrared properties, so it will not bias our results. In only one case, a SDSS source is located in the field of view of a Spitzer observation, but a counterpart was not detected. In that case, we estimate the corresponding upper limit as described below.

For our indicator of the nuclear luminosity, we used optical and UV (GALEX) data to estimate the bolometric luminosity individually for each source. Because the GALEX NUV band ( $1750\text{--}2800\text{ \AA}$ ) corresponds to  $875\text{--}1900\text{ \AA}$  in the rest-frame, we are able to measure directly the flux in much of the spectral peak region. The details of our method are presented in §2.5. In addition, we have also found it is sometimes convenient to use the SDSS i-band luminosity as a standard of comparison because in our redshift range it corresponds to rest-frame B-band.

### 2.1. SDSS Sample Data Collection

In order to construct a large sample of high luminosity unobscured quasars, we used the results from the Sloan Digital Sky Survey (SDSS; York et al. 2000), specifically from data release 5 (Adelman-McCarthy et al. 2006)<sup>4</sup>. Only sources classified as quasars by the SDSS pipeline, and thus presenting high-ionization broad emission lines, were considered. A detailed description of the SDSS quasar classification scheme was presented by Yip et al. (2004). There are 11937 SDSS/DR5 quasars in the  $0.8 \leq z \leq 1.2$  redshift range.

Spitzer data for these SDSS quasars were obtained from the archive using the Leopard v6.1 software<sup>5</sup>. A total of 638 Astronomical Observation Requests (AORs) were found with at least one source in our sample in the field. In many cases, these correspond to different observations of the same field, so only 206 quasars in our SDSS/DR5 sample were observed by Spitzer/MIPS. Only the post-BCD (Basic Calibrated Data) frames for

<sup>4</sup> Data available at <http://www.sdss.org/dr5>

<sup>5</sup> Leopard can be obtained at <http://ssc.spitzer.caltech.edu/propkit/spot/>

each AOR were downloaded. The Mosaicking and Point-source Extraction (MOPEX; Makovoz & Marleau 2005) package version 030106<sup>6</sup> was used in order to extract the sources and calculate fluxes from each AOR. The procedure described by Makovoz & Marleau (2005)<sup>7</sup>, was followed. Briefly, we did a first pass extraction including the brightest sources only, in order to calculate the point response function (PRF) for each mosaic. Using this specific PRF we then extracted sources with a signal-to-noise higher than 5. In the last step, the flux for each source was estimated by performing PRF fitting. In order to check this procedure, we downloaded the data from the Great Observatories Origins Deep Survey (GOODS; Dickinson et al. 2003) and compared the results obtained by following this procedure with those reported by the legacy survey team<sup>8</sup>. The flux densities presented in the GOODS catalog were converted into fluxes assuming a MIPS-24 bandwidth of  $4.7 \mu\text{m}$ , as reported by the MIPS data handbook. We found very good agreement between the two independent studies. On average, the fluxes reported by the GOODS team were higher by  $\sim 10\%$  with a spread of less than  $\sim 10\%$ , even after incorporating an aperture correction. Given that this small offset will not affect our results, we do not apply any correction to our fluxes.

The SDSS sample was then matched to the sources found in the Spitzer archive, using a maximum search radius of  $10''$ . This maximum nominal separation was chosen both to minimize the number of false counterparts and to take into account the positional uncertainties of both Spitzer and SDSS. Altogether, we found in these Spitzer images counterparts for 205 sources at a signal to noise higher than 5. In the remaining case, SDSS J024256.93-001558.0, a very faint counterpart is visible on the Spitzer image, but not significantly detected so we calculate a  $3\text{-}\sigma$  upper limit from the background standard deviation measured around the SDSS position. The distribution of distances between the SDSS position and the Spitzer counterpart can be seen in Figure 1. The average separation between the optical position and the IR counterpart was  $\sim 0.5''$ . For each SDSS source, we calculated the probability of a false match with a  $24 \mu\text{m}$  counterpart, assuming a Poissonian distribution of sources and the source density of the corresponding AOR. We found that the maximum probability of a false match for a given source was  $\sim 1.3\%$ , with an average probability of  $0.02\%$ .

The observed properties of these 206 sources can be found in Table 1. These objects were on average our most luminous, with bolometric luminosities ranging from  $2 \times 10^{45} \text{ erg s}^{-1}$  to  $3 \times 10^{47} \text{ erg s}^{-1}$ . Optical magnitudes in the AB system were obtained directly from the reported SDSS values. In all cases, the PSF fitting magnitude was used, as suggested by the SDSS team for sources that are unresolved at ground-based resolution. Although the errors in the SDSS photometry are negligible, since these are all relatively bright optical sources, errors in the MIPS-24  $\mu\text{m}$  photometry are estimated to be  $\sim 10\text{--}20\%$ , including both measurement and system-

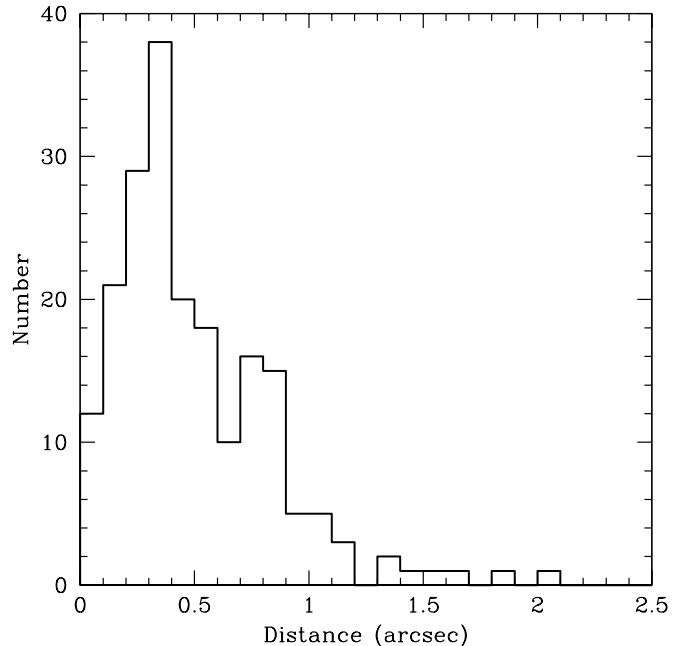


FIG. 1.— Distribution of distances between the optical position from the SDSS and the Spitzer MIPS counterpart. Average separation is  $0.5''$ .

atic ( $\sim 5\%$  according to the MIPS data handbook) uncertainties.

## 2.2. GOODS Sample Data Collection

In order to study lower luminosity sources, we include sources detected in both the north and south GOODS fields. A summary of the properties of these sources was presented by Treister et al. (2006). Our selection criteria were the same as for the SDSS sample: unobscured sources and  $0.8 < z < 1.2$ . In this case, a source was classified as unobscured if broad lines were present in the optical spectrum and the equivalent hydrogen column density of obscuration  $N_H$  in the X-ray spectrum was smaller than  $10^{22} \text{ cm}^{-2}$ . With these criteria, we found a total of 10 sources, 4 from the GOODS-N and 6 from the GOODS-S fields. These sources are in general intrinsically fainter than the SDSS sources, with bolometric luminosities ranging from  $1 \times 10^{44} \text{ erg s}^{-1}$  to  $1 \times 10^{46} \text{ erg s}^{-1}$ .

Optical magnitudes for these sources obtained from the Hubble Space telescope with the Advanced Camera for Surveys (ACS) imager were presented by the GOODS team (Giavalisco et al. 2004)<sup>9</sup>. In order to avoid problems related to the different spatial resolution of the GOODS and the SDSS images, we used aperture magnitudes with a  $2''$  diameter to calculate the optical fluxes of the GOODS sources.

The Spitzer properties and redshifts of these sources were obtained from the compilation of Treister et al. (2006), and are summarized in Table 2. The ID numbers in table 2 correspond to the X-ray identifications from the Alexander et al. (2003) catalog. Flux densities

<sup>6</sup> MOPEX can be downloaded from <http://ssc.spitzer.caltech.edu/postbcd/download-mopex.html>

<sup>7</sup> A more detailed description can be found at <http://ssc.spitzer.caltech.edu/postbcd/running-prf.html>

<sup>8</sup> The GOODS Spitzer data can be found at <http://data.spitzer.caltech.edu/popular/goods/>

<sup>9</sup> Available at [http://archive.stsci.edu/pub/hlsp/goods/catalog\\_r1/](http://archive.stsci.edu/pub/hlsp/goods/catalog_r1/)

in the 24  $\mu\text{m}$  band were converted into fluxes by multiplying them by the bandwidth of 4.7  $\mu\text{m}$ .

### 2.3. COSMOS Sample Data Collection

The COSMOS survey, covering a total area of 2  $\text{deg}^2$  at higher flux limits than GOODS, provides sources that fill the gap in luminosity between the SDSS and GOODS sources. Their span of luminosities is from  $2 \times 10^{44} \text{ erg s}^{-1}$  to  $1 \times 10^{46} \text{ erg s}^{-1}$ . We selected sources from this survey based on the optical spectroscopy observations of the XMM X-ray sources using the Magellan/IMACS multi-object spectrograph presented by Trump et al. (2006). Using our selection criteria ( $0.8 < z < 1.2$  and broad optical emission lines) we obtained a sample of 19 sources.

The COSMOS field was completely observed by Spitzer using both IRAC and MIPS as part of the S-COSMOS legacy program (Sanders et al. 2007). Using the public catalog of Spitzer sources generated by the COSMOS team<sup>10</sup>, we detected 14 of the 19 X-ray selected sources in the MIPS 24- $\mu\text{m}$  band. The observed properties of these sources are presented in Table 3. As for the GOODS sources, flux densities in the 24  $\mu\text{m}$  band were converted into fluxes by multiplying them by the bandwidth.

In summary, our sample consists of 230 sources spanning a range in bolometric luminosity from  $L_{\text{bol}} = 10^{44}$  to  $10^{47.5} \text{ erg s}^{-1}$ . All the sources in our sample have measured spectroscopic redshifts and present broad emission lines. In the IR, all these sources are bright, with luminosities from  $L_{\text{IR}} = 10^{43.5}$  to  $10^{46} \text{ ergs s}^{-1}$ .

### 2.4. GALEX Data

As a large fraction of the bolometric luminosity in unobscured AGN,  $\sim 15\text{--}20\%$ , can be found in the UV (e.g., Elvis et al. 1994; Richards et al. 2006; Trammell et al. 2007), it is worthwhile to look for UV counterparts of our sources in data taken by the Galaxy Evolution Explorer (GALEX; Martin et al. 2005). Specifically, we made use of data release 3<sup>11</sup>. In the case of the SDSS sources, we looked for UV counterparts in a  $10''$  radius around the optical position. The median separation over the whole sample was much less than the maximum permitted,  $\simeq 0.5''$ , and the actual maximum separation was only  $3.5''$ . 170 of the 206 sources in the SDSS sample were detected in at least one of the GALEX bands, for a detection rate of 83%. Of these 170 sources, 61 were detected only in the reddest NUV band and 4 detected only in the FUV band. The GALEX properties of the SDSS sources are presented in Table 1.

GALEX coverage of both GOODS fields is significantly deeper. Whereas the all-sky survey exposure time was only 0.1 ksec, the North field is being observed for 100 ksec as part of the deep imaging survey, and the South field is being observed for 200 ksec as part of the ultra-deep imaging survey. At the time of data release 2, the total time spent on the South field was only  $\sim 76$  ksec, while  $\sim 95$  ksec had been accumulated in the North field. Consequently, only 4 of the 6 sources in the South field were detected by GALEX, but all the sources in the North field have a UV counterpart. In Table 2, we present the GALEX properties of the GOODS

sources. The entire COSMOS field is one of the targets of the GALEX Ultra-Deep Imaging Survey. Hence, it is not surprising that all the sources in our sample with Spitzer-MIPS detections were also detected in the GALEX observations. The UV properties of the COSMOS sources are presented in Table 3.

### 2.5. Bolometric Luminosities

Because we believe the infrared continuum to be the result of reprocessing shorter wavelength radiation from the nucleus that strikes the dusty torus, including it in our estimate of the intrinsic nuclear bolometric luminosity when we have an unobscured view of the nucleus would be double-counting. Instead, we do the best we can to sum all flux from wavelengths shorter than  $\sim 1 \mu\text{m}$ ; the exact long wavelength cut-off is not important because the integral is in general dominated by the UV. We neglect X-ray contributions, but these are generally small,  $\lesssim 10\%$  (e.g., Richards et al. 2006).

In order to estimate the bolometric luminosities, we combined the photometric information from GALEX NUV (1750–2800 Å) to  $z$ -band ( $\sim 1 \mu\text{m}$ ). In the optical range, where there are only very small gaps in wavelength between the available photometric bands, we approximate the integrated luminosity by the sum of the observed luminosity in each band. For UV fluxes, we employ GALEX data wherever possible. Specifically, we use the GALEX NUV channel, which for our sample translates to rest-frame wavelengths 875–1400 Å. Whenever the object was either not observed by GALEX, or has only an upper bound, we estimate the flux in the NUV band by extrapolating from the bluest filter available ( $u$ -band for COSMOS and  $B$ -band for GOODS) using the median quasar SED from Richards et al. (2006). Both because GALEX data are missing from only a small fraction of our sample and because the intrinsic dispersion in bolometric corrections is  $\simeq 50\%$  (Richards et al. 2006), this extrapolation should not bias significantly our results. To account for the gap between the  $u$  band (rest-frame  $\sim 1750$  Å) and the GALEX NUV band, we linearly interpolate in  $F_\nu$ . At even shorter wavelengths, which are often not accessible in direct observations, we assume a power-law spectrum ( $f_\nu \propto \nu^\alpha$ ) with slope  $\alpha = -1.76$ , as reported by Telfer et al. (2002) in the 500–1200 Å regime. The amplitude of this power law is fixed by matching to either the GALEX photometry (when available) or the extrapolated flux from the SDSS composite spectrum when GALEX data are not available. From the templates of Richards et al. (2006), we estimate that  $\sim 20\%$  of the bolometric luminosity is emitted in this wavelength range.

The approach described above incorporates all the available information in the optical-UV range. In contrast, Maiolino et al. (2007) computed bolometric luminosities by multiplying the observed rest-frame 5100 Å luminosity by a fixed bolometric correction.

## 3. TRENDS

Our central result is shown in Figure 2. There we plot the ratio of MIPS 24  $\mu\text{m}$  luminosity,  $L_{\text{MIPS}}$ , to our estimate of the bolometric luminosity,  $L_{\text{bol}}$ , of each individual object. Two properties of the data are immediately apparent from this figure: that the mean value of this ratio decreases by order unity over the factor of 300 range

<sup>10</sup> Catalog available at <http://irsa.ipac.caltech.edu/Missions/cosmos.html>

<sup>11</sup> Available at <http://galex.stsci.edu/GR2/>

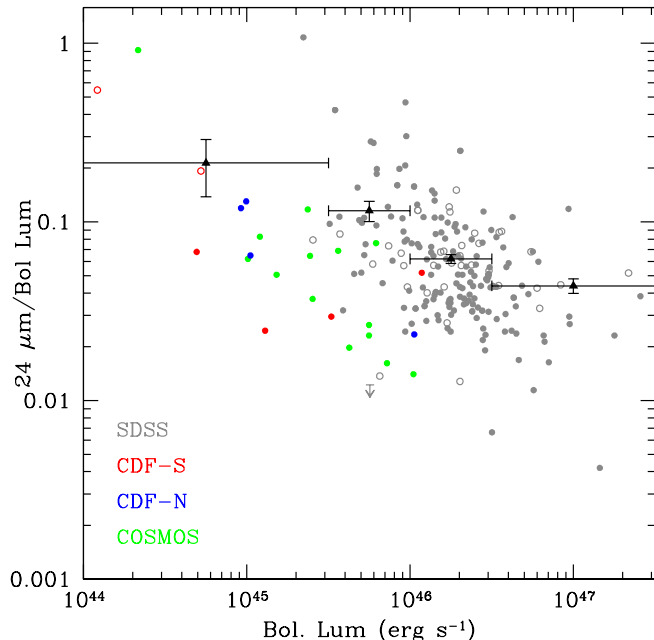


FIG. 2.— Ratio of 24  $\mu\text{m}$  to bolometric luminosity as a function of bolometric luminosity for all the sources in the sample. The open circles show the ratio for sources not detected by GALEX. Triangles with error bars show the average value in each luminosity bin, with 1- $\sigma$  vertical error bars.

in luminosity these data span; and that at any single luminosity there is a very large dispersion.

Although  $\langle L_{\text{MIPS}}/L_{\text{bol}} \rangle$  does change over this range of bolometric luminosities, it is not by a large factor: a factor of 3 is the best estimate. This figure may be compared with the factor of 2 contrast given by the fitting formula of Maiolino et al. (2007), meant to describe the sample means from  $\lambda L_{\lambda}(5100 \text{ \AA}) = 10^{43} \text{ ergs s}^{-1}$  to  $10^{47.5} \text{ ergs s}^{-1}$ , a somewhat greater dynamic range than spanned by our sample. Nonetheless, our sample size is large enough for the bin-means to be quite narrowly-defined, and the trend is clearly significant. Several statistical tests support this conclusion. To evaluate the significance in difference between the mean values in the two bins with the largest number of sample points (the second and third highest in luminosity), we apply Student's t-test; it shows that they are different at the 0.1% significance level, while the means of the highest and the third highest luminosity bins are different at the  $10^{-5}$  level. Similarly, the Spearman rank-correlation test finds that the correlation between  $\log(L_{\text{bol}})$  and  $\log(L_{\text{MIPS}}/L_{\text{bol}})$  is significant at the  $10^{-7}$  level. A conventional Pearson correlation test fails on these data because there are so many more SDSS quasars than COSMOS and GOODS sources, and the contrast in the mean infrared/bolometric luminosity across the narrower range of luminosity where most of the SDSS quasars are found is relatively small.

At the same time, the dispersion is very large. Considered in logarithmic terms, the rms fluctuation within the bins is 0.25–0.35, equivalent to a multiplicative factor of 1.8–2.2, comparable to the contrast in the mean across our entire luminosity range.

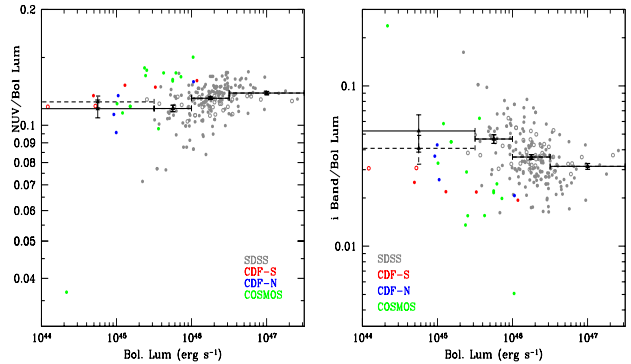


FIG. 3.— Same as Figure 2 but showing the GALEX NUV to bolometric luminosity (left panel) and  $i$ -band to bolometric luminosity (right panel) ratios as a function of bolometric luminosity. Dashed error bars show the mean values in the lowest luminosity bin if source COSMOS J100129.83+023239.0 is excluded.

That this trend (and large dispersion) is not related to effects in the intrinsic spectra of AGN can be seen by considering two other flux ratios as functions of  $L_{\text{bol}}$  (Fig. 3). In the mean, there is no significant change in the ratio of either the  $i$ -band luminosity or the NUV-band luminosity to bolometric. The small change observed in the  $i$ -band to bolometric luminosity ratio is heavily influenced by the single source COSMOS J100129.83+023239.0, which has a ratio  $\sim 8\times$  higher than the rest of the sources in that bin. If this source is removed, the average in the lower luminosity bin decreases from 0.052 to 0.041 and the trend disappears, as can be seen in Fig. 3. Performing a Spearman test, we found that the  $L_i/L_{\text{bol}}$  correlation with  $L_{\text{bol}}$  is  $\sim 3$  orders of magnitude less significant than the  $L_{\text{MIPS}}/L_{\text{bol}}$  correlation and has roughly the same significance as the  $L_{\text{NUV}}/L_{\text{bol}}$  correlation.

Moreover, there is far less intrinsic scatter at fixed  $L_{\text{bol}}$  in either of these ratios than in the infrared to bolometric ratio. The standard deviation of  $L_{\text{IR}}/L_{\text{bol}}$  in each luminosity bin is a factor of  $\sim 2.3$ , while for  $L_i/L_{\text{bol}}$ , it is  $\sim 1.5$  and for  $L_{\text{NUV}}/L_{\text{bol}}$  it is 1.12. The magnitude of the error induced by using a fixed bolometric correction to estimate bolometric luminosities from a given optical band is shown by the dispersion of the points plotted in both panels of Figure 3. Use of the  $i$ -band and a fixed bolometric correction, for example, entails an uncertainty in the bolometric luminosity of  $\sim 50\%$ .

#### 4. SIGNIFICANCE

##### 4.1. Evolution?

Just as it is possible that the physics controlling the geometry of obscuration is correlated in some way with the bolometric luminosity of the AGN, so too, it may change as a function of the age of the Universe. There is evidence, for example, that at fixed luminosity,  $f_{\text{obsc}}$  increases with increasing redshift (Treister & Urry 2006); this suggestion, however, remains controversial (e.g., Gilli et al. 2007). Factoring out any possible redshift-dependence was a strong motivating factor for our choice of a sample in which all the objects have approximately the same  $z$ .

In fact, the precise character of the correlation between  $f_{\text{obsc}}$  and  $L_{\text{bol}}$  also enters into the debate over the pos-

sible dependence of  $f_{\text{obsc}}$  on  $z$ . Currently-available samples that probe to high redshift are in general strongly incomplete at low luminosity because it is so difficult to obtain spectra for objects that faint. If one's estimate of the obscured fraction at high redshift is based solely on the detectable sources (which are, of course, high luminosity objects), it will be biased to a low value if  $f_{\text{obsc}}$  systematically declines with increasing luminosity at all redshifts.

#### 4.2. Relation between $L_{\text{MIPS}}/L_{\text{bol}}$ and the obscured solid angle

As we explained earlier, the ratio of infrared reprocessed light to bolometric luminosity should increase as the fraction of solid angle occupied by the dusty obscuring gas  $f_{\text{obsc}}$  increases. If the reprocessed IR were radiated isotropically, the ratio  $L_{\text{MIPS}}/L_{\text{bol}}$  would be proportional to  $f_{\text{obsc}}$ . It is much more likely, however, that the reradiation is anisotropic. Consequently, the relationship between these two quantities is not necessarily precisely linear, nor does it directly yield  $f_{\text{obsc}}$  without the introduction of any additional parameters (cf. Maiolino et al. 2007). At the very least (i.e., in the event of isotropic radiation), there is a proportionality constant to be determined.

At present, there are two lines of evidence regarding the directionality of the reradiated IR. On the observational side, there are suggestions that it may not be far from isotropic (Lutz et al. 2004; Horst et al. 2007). In both of these studies, it is claimed on the basis of small samples of AGN that the mean ratio of mid-IR flux to intrinsic hard X-ray flux is the same for both obscured and unobscured objects. However, in both of these studies, the intrinsic hard X-ray luminosities of the obscured objects are in general substantially smaller (by at least an order of magnitude) than those of the unobscured objects. Given the correlation we have found between  $L_{\text{MIPS}}/L_{\text{bol}}$  and  $L_{\text{bol}}$ , one might then have expected that in their samples the mid-IR to X-ray flux ratio would be even *higher* for the obscured than for the unobscured if the IR radiation were isotropic. We therefore do not regard these studies as making a strong case for isotropic radiation.

On the other hand, there are strong physical and theoretical arguments for thinking that the radiation is anisotropic. The obscuration is, after all, strongly aspherical—if it were otherwise, there would be very few unobscured objects to see. If the torus is optically thick in the radial direction in the mid-IR and that optical depth is larger than the vertical optical depth, most of the mid-IR flux should escape roughly parallel to the torus axis, with rather less escaping in the equatorial direction. Every detailed radiation transfer model published shows this tendency, although the precise contrast between the  $12\mu\text{m}$  flux toward the pole and toward the equator varies depending on the details of the adopted density distribution (Pier & Krolik 1993; Granato & Danese 1994; Efstathiou & Rowan-Robinson 1995; Nenkova et al. 2002; van Bemmél & Dullemond 2003; Dullemond & van Bemmél 2005). The most recent paper (which presents both smooth and clumpy models) finds ratios between the total infrared flux in the equatorial plane and at  $20^\circ$  from the axis to vary between 0.06 and 0.3, depending on the specific model. Making

the approximation that very little flux is directed toward observers in the obscured solid angle, we expect that the MIPS-band luminosity should scale relative to the bolometric luminosity approximately as

$$\frac{dL_{\text{MIPS}}}{d\Omega} \simeq f_{12}(\theta) \frac{L_{\text{bol}}}{4\pi} \frac{f_{\text{obsc}}}{1 - f_{\text{obsc}}}. \quad (1)$$

Here  $f_{12}(\theta)$  is the fraction of the total dust-reprocessed luminosity falling within the MIPS band ( $\simeq 11\text{--}13\mu\text{m}$  in the rest-frame at  $z \simeq 1$ ). Even within the range of viewing angles  $\theta$  that provide an unobscured view, we may expect order unity variations in this quantity.

To confirm this scaling and estimate  $f_{12}(\theta)$ , we studied the results of a number of model calculations. These models were performed with the code described in Dullemond & van Bemmél (2005). For all of them, the obscuration was assumed to be confined to within a constant opening-angle spherical wedge whose outer radius was 30 times greater than its inner radius. We considered two density profiles: a single constant value and a radial decay  $\propto r^{-1}$ . For both density models, when the torus is optically thick in the mid-infrared, the approximate model given by equation 1 is confirmed provided the opening angle is at least  $\simeq 0.7$  radians. Crudely speaking, the solid angle-weighted mean value of  $f_{12}$  (for viewing angles permitting an unobscured view of the nucleus) does not vary a great deal with torus opening angle: it varies from  $\simeq 0.06$  to  $\simeq 0.08$  depending on the model details for the same range of opening angles for which equation 1 holds. When the opening angle becomes smaller than this,  $f_{12}$  can begin to diminish, with the amount sensitive to whether the torus is truly a spherical wedge or has a flatter outer envelope. At fixed opening angle,  $f_{12}$  does vary somewhat with viewing angle, typically being perhaps 50% greater than the mean for nearly polar viewing angle and dropping sharply when the viewing angle becomes close to the torus opening angle. The latter effect is also sensitive to the specific geometry (spherical wedge) adopted in these models, which also depends slightly on the wavelength of the emission.

The ratio of IR flux to bolometric seen by an observer in the unobscured direction is then

$$\frac{L_{\text{MIPS}}}{L_{\text{bol}}} \simeq f_{12}(\theta) \frac{f_{\text{obsc}}}{1 - f_{\text{obsc}}}. \quad (2)$$

To this level of approximation, the obscured fraction associated with a given value of  $L_{\text{MIPS}}/L_{\text{bol}}$  is

$$f_{\text{obsc}} \simeq \frac{1}{1 + q}, \quad (3)$$

where

$$q = \frac{f_{12}(\theta)}{L_{\text{MIPS}}/L_{\text{bol}}}. \quad (4)$$

Using the solid angle-weighted means of  $f_{12}$  taken from our models, we can transform the bin-means of  $L_{\text{MIPS}}/L_{\text{bol}}$  shown in Figure 2 to estimates of  $f_{\text{obsc}}$ . The results are shown in Figure 4. It appears that the mean value of  $f_{\text{obsc}}$  falls from  $\simeq 0.9$  at the lowest bolometric luminosities in our sample to  $\simeq 0.3\text{--}0.4$  at the highest luminosities. *We strongly caution, however, that there may be a systematic error of order unity in  $\langle f_{12} \rangle$  due to the specific assumptions made in those models regarding*

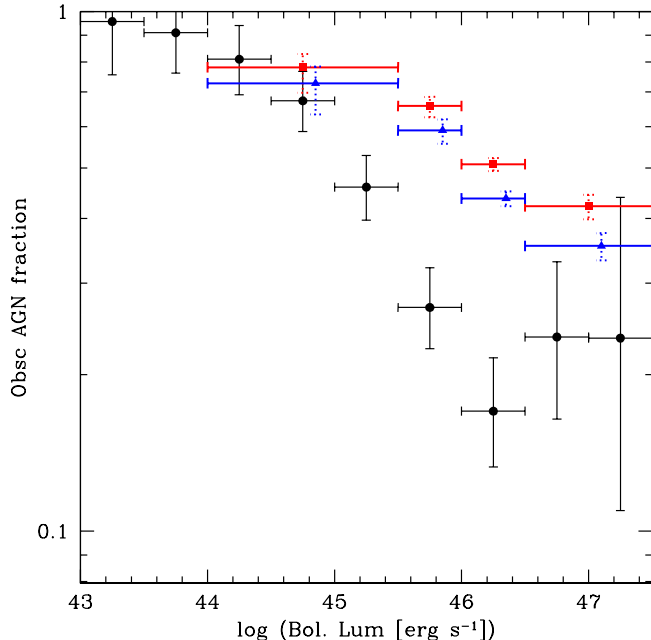


FIG. 4.— Two different inferences of  $f_{\text{obsc}}$ : black curve with error bars from X-ray data, as described in the text; triangles with error bars from the method of this paper assuming values of  $f_{12}=0.06$  (squares; red in electronic version) and 0.08 (triangles; blue in electronic version; displaced by  $\log L_{\text{bol}}=0.1$  for clarity). The horizontal error bars simply describe the width of the luminosity bin; the vertical red and blue error bars are dashed to indicate that they are model-dependent in the sense discussed in the text. Their extent was determined by translating the error bars of Fig. 2 using Eqn. 3.

the density distribution within the envelope that determines  $f_{\text{obsc}}$ . A variety of parameters (e.g., the ratio of outer radius to inner, the degree of inhomogeneity and clumping, etc.) may quantitatively alter  $\langle f_{12} \rangle$ .

We compare this dependence of the mean  $f_{\text{obsc}}$  as a function of  $L_{\text{bol}}$  with the relation that has been found in X-ray studies in Figure 4. For this figure we use the X-ray sample of Treister & Urry (2006), with the X-ray luminosity transformed to  $L_{\text{bol}}$  using the luminosity-dependent bolometric corrections of Marconi et al. (2004). The level of agreement between the two independent methods of inferring  $f_{\text{obsc}}$  is surprisingly good, considering the systematic errors in both. Most notably, X-ray surveys completely miss objects with column densities  $\gg 10^{24} \text{ cm}^{-2}$ , and there are indications that these objects may be numerous (Martínez-Sansigre et al. 2006; Polletta et al. 2006). Indeed, if one wished to extend credence to the somewhat larger  $f_{\text{obsc}}$  found by the infrared method at intermediate luminosities, it might be explained by a somewhat larger proportion of Compton-thick objects within the population. It is also interesting that, as pointed out by Maiolino et al. (2007), the values of  $f_{\text{obsc}}$  derived from X-ray surveys include the effects of obscuration by both dust and gas, while the IR-derived values include only obscuration by dust.

To close this subsection, we remark on another distinction that may be important in evaluating the mean-

ing of the  $f_{\text{obsc}}$  estimated from  $L_{\text{MIPS}}/L_{\text{bol}}$ . It is possible for obscuring matter of smaller optical depth to intercept some of the nuclear light farther out in the host galaxy and reradiate it in the mid-infrared even though this matter is wholly independent of the “obscuring torus” proper (e.g., Keel 1980; McLeod & Rieke 1995; Rigby et al. 2006). Molecular clouds and other gas concentrations in the host have at most modest column densities when measured in terms of X-ray absorption (generally  $< 10^{22} \text{ cm}^{-2}$ ), but such column densities can still absorb large portions of an AGN’s optical/UV continuum. Consequently, they qualify as contributing to  $f_{\text{obsc}}$  both in the sense that they can block our view of the optical/UV light from the nucleus and, depending on their temperature, in terms of their contribution to the mid-infrared luminosity of the system.

#### 4.3. The dispersion at fixed luminosity

One of the virtues of using SDSS quasars is that the sample size, particularly for  $5 \times 10^{45} \text{ erg s}^{-1} < L_{\text{bol}} < 1 \times 10^{47} \text{ erg s}^{-1}$ , is large enough to be truly statistical. As a result, we can obtain a reasonably reliable estimate of the sample dispersion as well as its mean. As we have previously remarked, the dispersion is quite large.

We see no measurement error that could contribute in a significant way to the dispersion in  $L_{\text{MIPS}}/L_{\text{bol}}$  at fixed  $L_{\text{bol}}$ . The errors in the photometry we use to compute the bolometric luminosity are small,  $\sim 2\%$ ; the uncertainty in the MIPS fluxes is  $\sim 10\text{--}20\%$ , as detailed in §2.1.

Intrinsic variability could also contribute, but in a similarly minor fashion except perhaps in a very small number of objects. The time interval between the GALEX measurements, the SDSS photometry, and the Spitzer measurements was generally a few years. On that timescale, SDSS data (Vanden Berk et al. 2004) show that quasars typically vary by 0.1–0.2 mag in the optical, with the larger variability usually occurring at shorter wavelengths and in lower luminosity objects. A small fraction vary by as much as  $\simeq 0.5$  mag on these timescales, still much smaller than our observed dispersion relative to the mean. If the infrared is, as we assume, the result of thermal reprocessing by dust, it cannot vary substantially on timescales shorter than several to ten years.

According to the results of Schweitzer et al. (2006), the contribution of star formation to the total light in quasars is  $\sim 30\%$  at far-IR wavelengths, in agreement with the results of Shi et al. (2007), who found a contribution of  $\sim 25\%$  at  $70 \mu\text{m}$  and  $\sim 10\%$  at  $24 \mu\text{m}$ . Hence, extrapolating linearly to the MIPS band, we expect a contribution of star formation to the total IR light of  $\sim 5\%$  at rest-frame  $12 \mu\text{m}$ ; we therefore do not expect our results to be significantly affected by star formation processes in the host galaxy. In addition, because  $f_{\text{obsc}}$  is larger for lower luminosity sources than for higher luminosity sources and the nuclear infrared luminosity is  $f_{\text{obsc}} L_{\text{bol}}$ , we do not expect the contribution from star formation to increase significantly even at lower luminosities.

There must, therefore, be a genuine large dispersion in  $L_{\text{MIPS}}/L_{\text{bol}}$ . One possible source of this dispersion is the variation of  $f_{12}$  with viewing angle. Again relying on the models described above, a total range of a factor of 2–3 may be expected from this source alone. Compared with



our rms logarithmic dispersion of a factor of  $\sim 2$ , or the factor of 100 total range seen in the most-populated bins, the expected variations in viewing angle can account for a significant part of this dispersion, but likely not all of it.

This last statement must, of course, be qualified by the condition that our models accurately estimate the range in  $f_{12}(\theta)$ . It is entirely possible that changes in the detailed density distribution, even while keeping  $f_{\text{obsc}}$  fixed, might introduce further variations in  $f_{12}(\theta)$ . Although the expected large optical depth in the  $12\mu\text{m}$  band is likely to limit the sensitivity of  $f_{12}(\theta)$  to changes in the radial density profile or density inhomogeneities, there could certainly be small, but detectable, quantitative effects.

Finally, there may, of course, be additional dispersion due to variations in  $f_{\text{obsc}}$  at fixed luminosity. It is entirely possible for parameters other than  $L_{\text{bol}}$  to influence the obscuration's solid angle. Among the obvious candidates are the mass of the central mass black hole and the stellar mass contained within the region of the obscuring matter. The varying impact of magnetic forces, clump collisions, or other mechanisms could also conceivably play a part.

#### 4.4. Implications for surveys

Particularly since the launch of the *Spitzer Space Telescope*, it has become feasible—and worthwhile—to construct samples of AGN based on mid-infrared selection (Lacy et al. 2004; Stern et al. 2005; Martínez-Sansigre et al. 2006). Our results here demonstrate that the translation between mid-infrared flux and bolometric flux has an intrinsic scatter of a factor of  $\simeq 2$  up or down, even for unobscured AGN. Because, as we have discussed,  $L_{\text{IR}}/L_{\text{bol}}$  is generally smaller in obscured AGN than in unobscured, the bolometric correction based on infrared flux for them should be an even larger factor, with perhaps greater scatter.

#### 5. CONCLUSIONS

We presented in this paper an alternative way to estimate the fraction of obscured AGN and its possible dependence on luminosity, by computing the relative fraction of IR emission in unobscured AGN spanning a large of luminosities. Using a sample of 206 optically-selected high luminosity AGN from the SDSS and 24 X-ray selected lower luminosity AGN from the GOODS and COS-

MOS surveys with  $0.8 \leq z \leq 1.2$ , nearly all having Spitzer detections at  $24\mu\text{m}$ , we found a decrease of a factor of  $\sim 3$  in the relative IR emission at rest-frame  $12\mu\text{m}$  from  $L_{\text{bol}} = 10^{44} \text{ ergs s}^{-1}$  to  $10^{47.5} \text{ ergs s}^{-1}$ . In addition, we found a significant scatter of a factor of 2–3 at a given bolometric luminosity. Some of this scatter can likely be explained by a dependence of the  $11\text{--}13\mu\text{m}$  fraction  $f_{12}$  on viewing angle; some may also be due to an intrinsic scatter in  $f_{\text{obsc}}$  at fixed bolometric luminosity due to a dependence on other parameters such as black hole mass, magnetic forces, etc.

Using IR re-emission models in order to convert  $L_{\text{MIPS}}/L_{\text{bol}}$  into a fraction of obscured AGN, we found that  $f_{\text{obsc}}$  changes from  $\sim 90\%$  at  $L_{\text{bol}} = 10^{44} \text{ ergs s}^{-1}$  to  $\sim 30\text{--}40\%$  at  $L_{\text{bol}} \simeq 10^{47} \text{ ergs s}^{-1}$ . The derived dependence of the obscured fraction on luminosity is in good agreement with the direct, but possibly biased (by the omission of Compton-thick objects) observation of this fraction in X-ray surveys. We caution, however, that there may be systematic error in the precise values of  $f_{\text{obsc}}$  inferred from  $L_{\text{MIPS}}/L_{\text{bol}}$  because our estimate of  $\langle f_{12} \rangle$  is likely to depend somewhat on the details of the density distribution within the torus. Nonetheless, it is interesting that in general the values of  $f_{\text{obsc}}$  we infer are larger than what is seen in X-ray surveys. This contrast hints that there may be a significant population of heavily obscured, even Compton thick, AGN that are missed in X-ray observations but included in our samples.

We thank ESO-Chile for JHK's support through its senior visitor program, and the hospitality given him during his visit to Santiago. We thank the anonymous referee for very useful comments and suggestions. This work is based in part on archival data obtained with the Spitzer Space Telescope, which is operated by the Jet Propulsion Laboratory, California Institute of Technology under a contract with NASA. It was partially supported by a Spitzer Archival Research grant, subcontract number 1310126 from Caltech/JPL. Funding for the SDSS and SDSS-II has been provided by the Alfred P. Sloan Foundation, the Participating Institutions, the National Science Foundation, the U.S. Department of Energy, the National Aeronautics and Space Administration, the Japanese Monbukagakusho, the Max Planck Society, and the Higher Education Funding Council for England. The SDSS Web Site is <http://www.sdss.org/>.

#### REFERENCES

- Adelman-McCarthy, J. K. et al. 2006, *ApJS*, 162, 38  
 Alexander, D. M., Bauer, F. E., Brandt, W. N., Schneider, D. P., Hornschemeier, A. E., Vignali, C., Barger, A. J., Broos, P. S., Cowie, L. L., Garmire, G. P., Townsley, L. K., Bautz, M. W., Chartas, G., & Sargent, W. L. W. 2003, *AJ*, 126, 539  
 Alonso-Herrero, A., Pérez-González, P. G., Alexander, D. M., Rieke, G. H., Rigopoulou, D., Le Floc'h, E., Barmby, P., Papovich, C., Rigby, J. R., Bauer, F. E., Brandt, W. N., Egami, E., Willner, S. P., Dole, H., & Huang, J.-S. 2006, *ApJ*, 640, 167  
 Antonucci, R. 1993, *ARA&A*, 31, 473  
 Antonucci, R. R. J. & Miller, J. S. 1985, *ApJ*, 297, 621  
 Barger, A. J., Cowie, L. L., Mushotzky, R. F., Yang, Y., Wang, W.-H., Steffen, A. T., & Capak, P. 2005, *AJ*, 129, 578  
 di Serego Alighieri, S., Cimatti, A., & Fosbury, R. A. E. 1994, *ApJ*, 431, 123  
 Dickinson, M., Giavalisco, M., & The GOODS Team. 2003, in *The Mass of Galaxies at Low and High Redshift*, ed. R. Bender & A. Renzini, 324–+  
 Dullemond, C. P. & van Bemmelen, I. M. 2005, *A&A*, 436, 47  
 Efstathiou, A. & Rowan-Robinson, M. 1995, *MNRAS*, 273, 649  
 Elvis, M., Wilkes, B. J., McDowell, J. C., Green, R. F., Bechtold, J., Willner, S. P., Oey, M. S., Polonski, E., & Cutri, R. 1994, *ApJS*, 95, 1  
 Ferruit, P., Wilson, A. S., & Mulchaey, J. 2000, *ApJS*, 128, 139  
 Giavalisco, M. et al. 2004, *ApJ*, 600, L93  
 Gilli, R., Comastri, A., & Hasinger, G. 2007, *A&A*, 463, 79  
 Granato, G. L. & Danese, L. 1994, *MNRAS*, 268, 235  
 Hao, L., Strauss, M. A., Fan, X., Tremonti, C. A., Schlegel, D. J., Heckman, T. M., Kauffmann, G., Blanton, M. R., Gunn, J. E., Hall, P. B., Ivezić, Ž., Knapp, G. R., Krolik, J. H., Lupton, R. H., Richards, G. T., Schneider, D. P., Strateva, I. V., Zakamska, N. L., Brinkmann, J., & Szokoly, G. P. 2005, *AJ*, 129, 1795



- Horst, H., Gandhi, P., Smette, A. & Duschl, W.J. 2007, A&A in press, arXiv:0711.3734
- Jaffe, W., Meisenheimer, K., Röttgering, H. J. A., Leinert, C., Richichi, A., Chesneau, O., Fraix-Burnet, D., Glazeborg-Kluttig, A., Granato, G.-L., Graser, U., Heijligers, B., Köhler, R., Malbet, F., Miley, G. K., Paresce, F., Pel, J.-W., Perrin, G., Przygodda, F., Schoeller, M., Sol, H., Waters, L. B. F. M., Weigelt, G., Woillez, J., & de Zeeuw, P. T. 2004, *Nature*, 429, 47
- Keel, W. C. 1980, *AJ*, 85, 198
- Krolik, J. H. 1999, *Active galactic nuclei : from the central black hole to the galactic environment (Active galactic nuclei : from the central black hole to the galactic environment / Julian H. Krolik. Princeton, N. J. : Princeton University Press, c1999.)*
- La Franca, F., et al. 2005, *ApJ*, 635, 864
- Lacy, M., Petric, A. O., Sajina, A., Canalizo, G., Storrie-Lombardi, L. J., Armus, L., Fadda, D., & Marleau, F. R. 2007, *AJ*, 133, 186
- Lacy, M., et al. 2004, *ApJS*, 154, 166
- Lawrence, A. 1991, *MNRAS*, 252, 586
- Lutz, D., Maiolino, R., Spoon, H.W.W. & Moorhead, A.F.M. 2004, *A&A*, 418, 465
- Maiolino, R., Shemmer, O., Imanishi, M., Netzer, H., Oliva, E., Lutz, D., & Sturm, E. 2007, *A&A*, 468, 979
- Makovoz, D. & Marleau, F. R. 2005, *PASP*, 117, 1113
- Marconi, A., Risaliti, G., Gilli, R., Hunt, L. K., Maiolino, R., & Salvati, M. 2004, *MNRAS*, 351, 169
- Martin, D. C. et al. 2005, *ApJ*, 619, L1
- Martínez-Sansigre, A., Rawlings, S., Lacy, M., Fadda, D., Jarvis, M. J., Marleau, F. R., Simpson, C., & Willott, C. J. 2006, *MNRAS*, 370, 1479
- McLeod, K. K. & Rieke, G. H. 1995, *ApJ*, 441, 96
- Nenkova, M., Ivezić, Ž., & Elitzur, M. 2002, *ApJ*, 570, L9
- Pier, E. A. & Krolik, J. H. 1992, *ApJ*, 401, 99
- . 1993, *ApJ*, 418, 673
- Polletta, M. d. C., et al. 2006, *ApJ*, 642, 673
- Richards, G. T., Lacy, M., Storrie-Lombardi, L. J., Hall, P. B., Gallagher, S. C., Hines, D. C., Fan, X., Papovich, C., Vanden Berk, D. E., Trammell, G. B., Schneider, D. P., Vestergaard, M., York, D. G., Jester, S., Anderson, S. F., Budavári, T., & Szalay, A. S. 2006, *ApJS*, 166, 470
- Rigby, J. R., Rieke, G. H., Donley, J. L., Alonso-Herrero, A., & Pérez-González, P. G. 2006, *ApJ*, 645, 115
- Risaliti, G., Maiolino, R., & Salvati, M. 1999, *ApJ*, 522, 157
- Sanders, D. B., et al. 2007, *ApJS*, 172, 86
- Schmitt, H. R., Donley, J. L., Antonucci, R. R. J., Hutchings, J. B., & Kinney, A. L. 2003, *ApJS*, 148, 327
- Schweitzer, M., et al. 2006, *ApJ*, 649, 79
- Shi, Y., et al. 2007, *ApJ*, 669, 841
- Simpson, C. 2005, *MNRAS*, 360, 565
- Spergel, D. N., Bean, R., Doré, O., Nolte, M. R., Bennett, C. L., Dunkley, J., Hinshaw, G., Jarosik, N., Komatsu, E., Page, L., Peiris, H. V., Verde, L., Halpern, M., Hill, R. S., Kogut, A., Limon, M., Meyer, S. S., Odegard, N., Tucker, G. S., Weiland, J. L., Wollack, E., & Wright, E. L. 2007, *ApJS*, 170, 377
- Steffen, A. T., Barger, A. J., Cowie, L. L., Mushotzky, R. F., & Yang, Y. 2003, *ApJ*, 596, L23
- Stern, D., Eisenhardt, P., Gorjian, V., Kochanek, C. S., Caldwell, N., Eisenstein, D., Brodwin, M., Brown, M. J. I., Cool, R., Dey, A., Green, P., Jannuzi, B. T., Murray, S. S., Pahre, M. A., & Willner, S. P. 2005, *ApJ*, 631, 163
- Telfer, R. C., Zheng, W., Kriss, G. A., & Davidsen, A. F. 2002, *ApJ*, 565, 773
- Trammell, G. B., Vanden Berk, D. E., Schneider, D. P., Richards, G. T., Hall, P. B., Anderson, S. F., & Brinkmann, J. 2007, *AJ*, 133, 1780
- Treister, E. & Urry, C. M. 2006, *ApJ*, 652, L79
- Treister, E., Urry, C. M., Van Duyn, J., Dickinson, M., Chary, R.-R., Alexander, D. M., Bauer, F., Natarajan, P., Lira, P., & Grogan, N. A. 2006, *ApJ*, 640, 603
- Treister, E. et al. 2004, *ApJ*, 616, 123
- Tristram, K. R. W., Meisenheimer, K., Jaffe, W., Schartmann, M., Rix, H. ., Leinert, C., Morel, S., Wittkowski, M., Röttgering, H., Perrin, G., Lopez, B., Raban, D., Cotton, W. D., Graser, U., Paresce, F., & Henning, T. 2007, *A&A* in press, arXiv:0709.0209
- Trump, J. R., Impey, C. D., McCarthy, P. J., Elvis, M., Huchra, J. P., Brusa, M., Hasinger, G., Schinnerer, E., Capak, P., Lilly, S. J., & Scoville, N. Z. 2006, *ArXiv Astrophysics e-prints*
- Ueda, Y., Akiyama, M., Ohta, K., & Miyaji, T. 2003, *ApJ*, 598, 886
- van Bemmell, I. M. & Dullemond, C. P. 2003, *A&A*, 404, 1
- Vanden Berk, D. E., Willite, B. C., Kron, R. G., Anderson, S. F., Brunner, R. J., Hall, P. B., Ivezić, Ž., Richards, G. T., Schneider, D. P., York, D. G., Brinkmann, J. V., Lamb, D. Q., Nichol, R. C., & Schlegel, D. J. 2004, *ApJ*, 601, 692
- Yip, C. W., Connolly, A. J., Vanden Berk, D. E., Ma, Z., Frieman, J. A., SubbaRao, M., Szalay, A. S., Richards, G. T., Hall, P. B., Schneider, D. P., Hopkins, A. M., Trump, J., & Brinkmann, J. 2004, *AJ*, 128, 2603
- York, D. G. et al. 2000, *AJ*, 120, 1579
- Zakamska, N. L., Strauss, M. A., Krolik, J. H., Collinge, M. J., Hall, P. B., Hao, L., Heckman, T. M., Ivezić, Ž., Richards, G. T., Schlegel, D. J., Schneider, D. P., Strateva, I., Vanden Berk, D. E., Anderson, S. F., & Brinkmann, J. 2003, *AJ*, 126, 2125

TABLE 1  
OBSERVED PROPERTIES OF SOURCES IN THE SDSS SAMPLE

Name	Redshift	Optical Mag. (AB)					$z$	Flux ( $10^{-12}$ erg cm $^{-2}$ s $^{-1}$ )						log(Bol. Lum) erg s $^{-1}$
		$u$	$g$	$r$	$i$			24 $\mu$ m flux	NUV flux	upper	lower	flux	FUV upper	lower
SDSS J110116.41+572850.5	0.80	17.85	17.53	17.48	17.46	17.40	0.331	1.335	1.341	1.332	0.466	0.470	0.462	46.5
SDSS J142810.31+353847.0	0.80	19.09	18.79	18.74	18.89	18.71	0.120	0.431	0.436	0.426	0.179	—	—	46.0
SDSS J104755.02+120850.2	0.81	19.84	19.43	19.16	19.02	18.71	0.537	0.202	0.214	0.191	0.012	0.016	0.008	45.8
SDSS J143345.10+345939.9	0.81	20.36	19.64	19.10	18.84	18.49	0.485	0.089	0.091	0.086	0.055	—	—	45.5
SDSS J160630.60+542007.5	0.82	19.03	18.77	18.73	18.83	18.61	0.413	0.455	0.459	0.452	0.185	—	—	46.1
SDSS J235948.53-103938.5	0.83	18.07	17.87	17.79	17.80	17.71	0.439	1.209	1.226	1.190	0.421	0.436	0.407	46.5

NOTE. — This table is published in its entirety in the electronic edition of the Astrophysical Journal. A portion is shown here for guidance regarding its form and content.

TABLE 2  
OBSERVED PROPERTIES OF SOURCES IN THE GOODS SAMPLE

Field	ID	Redshift	Optical Mag. (AB)				$z$	Flux ( $10^{-12}$ erg cm $^{-2}$ s $^{-1}$ )						log(Bol. Lum) erg s $^{-1}$
			$B$	$V$	$i$			24 $\mu$ m flux	NUV flux	upper	lower	flux	FUV upper	lower
South	34	1.040	22.72	22.36	22.23	21.23	0.006	0.029	0.030	0.028	0.006	0.007	0.006	45.1
South	173	1.030	20.17	20.00	19.94	19.03	0.112	0.281	0.283	0.280	0.092	0.093	0.091	46.1
South	214	0.840	24.09	23.47	22.56	21.34	0.010	0.018	0.020	0.016	0.009	0.011	0.008	44.7
South	234	0.840	20.95	20.54	20.65	19.65	0.029	0.125	0.126	0.124	0.038	0.039	0.037	45.5
South	193	0.960	23.71	23.16	22.63	21.40	0.022	0.013	—	—	0.005	—	—	44.7
South	200	0.960	25.49	24.89	24.22	22.92	0.014	0.003	—	—	0.001	—	—	44.1
North	116	1.022	22.62	22.08	22.00	20.88	0.021	0.018	0.019	0.018	0.008	—	—	45.0
North	340	0.903	22.91	22.20	21.89	20.75	0.017	0.032	0.033	0.031	0.009	—	—	45.0
North	344	1.018	20.13	19.89	19.95	19.15	0.047	0.259	0.260	0.258	0.050	—	—	46.0
North	451	0.837	28.47	21.33	21.21	20.09	0.039	0.029	0.030	0.028	0.019	—	—	45.0

TABLE 3  
OBSERVED PROPERTIES OF SOURCES IN THE COSMOS SAMPLE

Name	Redshift	Optical Mag. (AB)					$z$	Flux ( $10^{-12}$ erg cm $^{-2}$ s $^{-1}$ )						log(Bol. Lum) erg s $^{-1}$
		$u$	$g$	$r$	$i$			24 $\mu$ m flux	NUV flux	upper	lower	flux	FUV upper	lower
COSMOS J095902.56+022511.8	1.105	22.39	22.69	22.42	22.23	21.06	0.010	0.018	0.021	0.015	0.007	—	—	45.0
COSMOS J095940.06+022306.8	1.132	20.92	20.62	20.29	20.22	20.35	0.036	0.051	0.078	0.034	0.026	—	—	45.6
COSMOS J095946.92+022209.5	0.909	22.07	21.87	21.64	21.76	22.71	0.069	0.083	0.084	0.082	0.026	0.027	0.025	45.4
COSMOS J100033.38+015237.2	0.831	21.17	20.83	20.74	20.73	20.07	0.026	0.180	0.215	0.152	0.026	—	—	45.6
COSMOS J100034.93+020235.2	1.177	21.14	21.40	21.05	20.98	20.51	0.020	0.096	0.097	0.095	0.030	0.031	0.029	45.7
COSMOS J100042.37+014534.1	1.161	22.54	22.88	22.27	21.86	20.84	0.020	0.215	0.275	0.167	0.006	—	—	46.0
COSMOS J100049.97+015231.3	1.156	21.21	21.27	21.00	20.96	20.65	0.018	0.101	0.103	0.100	0.038	0.039	0.037	45.7
COSMOS J100114.86+020208.8	0.989	21.91	21.82	21.42	21.13	21.12	0.020	0.026	0.042	0.016	0.011	—	—	45.1
COSMOS J100118.57+022739.4	1.052	22.07	21.26	20.64	20.46	20.24	0.082	0.147	0.208	0.104	0.009	—	—	45.8
COSMOS J100129.83+023239.0	0.825	24.80	22.72	21.66	20.99	20.88	0.062	0.003	—	—	0.004	0.005	0.003	44.3
COSMOS J100141.33+021031.5	0.982	22.29	21.96	21.39	21.10	21.44	0.032	0.068	0.069	0.066	0.014	0.015	0.013	45.4
COSMOS J100151.11+020032.7	0.964	20.59	20.49	20.26	20.29	20.21	0.025	0.208	0.212	0.203	0.079	0.082	0.076	45.9
COSMOS J100159.86+013135.3	0.977	22.31	21.96	21.73	21.73	21.45	0.020	0.073	0.075	0.072	0.037	0.038	0.036	45.4
COSMOS J100229.33+014528.1	0.876	21.90	21.25	20.77	20.84	20.39	0.021	0.047	0.047	0.046	0.027	0.028	0.026	45.2